Sustainable Structures
ISSN: 2789-3111 (Print); ISSN: 2789-312X (Online)
http://www.sustain-dpl.com/journal/sust
DOI: 10.54113/j.sust.2025.000070

ORIGINAL ARTICLE

Experimental and numerical study on the flexural performance of reinforced laminated bamboo lumber beams with prestressed GFRP bars

Haitao Li[a,b,c,*], Dong Yang[a,b,c], Ben Chen[a,b,c], Sarah Mohrmann[a,b,c], Rodolfo Lorenzo[d], Kun Zhou[e], Feng Shen[f]

[a] College of Civil Engineering, Nanjing Forestry University, Nanjing 210037, China
[b] Jiangsu Carbon Sequestration Materials and Structural Technology of Bamboo & Wood Research Center, Nanjing Forestry University, Nanjing 210037, China
[c] National-provincial joint engineering research center of biomaterials for MACHINERY PACKAGE, Nanjing Forestry University, Nanjing 210037, China
[d] University College London, London WC1E 6BT, UK
[e] Guangxi Lvjing Bamboo Industry Co., LTD, 541402, China
[f] Jiangsu Fiber Composite Co., Ltd., Yancheng, 224700, China
[*]Corresponding Author: Haitao Li, Professor, E-mail: lhaitao1982@126.com

Abstract: This paper presents a new method to strengthen laminated bamboo lumber (LBL) beam by embedding prestressed glass fiber reinforced polymer (GFRP) bars at the bottom of LBL beams. The bending test of 30 LBL beams with a size of 2000 mm × 100 mm × 150 mm was carried out with the prestress level and reinforcement ratio as the influencing factors. The test result shows that the failure mode of prestressed LBL beams is mainly the fracture of bamboo fibers at the bottom of the beams. Embedding prestressed GFRP bars in the specimens is a good way to enhance the mechanical properties of LBL beams, including flexural capacity and stiffness. The ultimate bearing capacity of prestressed GFRP bars composited beams are increased to 40.6%, and the bending stiffness are increased by 22.5% comparing with ordinary beams. Based on the test results, a theoretical calculation model for the bearing capacity of the LBL beam was finally proposed, and the calculation results were basically consistent with the experimental results. Finite element modelling (FEM) using continuum damage mechanics was also adopted to verify the failure pattern and the strengthening mechanism of strengthened LBL beams.

Keywords: Laminated bamboo lumber beams, GFRP bars, prestress, flexural capacity, bending stiffness

1 Introduction

As the concept of green environmental protection has taken root in people's hearts, wood and bamboo have gradually become popular green building materials. Similar to wood [1-4], bamboo has a long history of use as a building material [5-7], and the production cycle of raw bamboo is significantly lower than that of wood [8-10]. However, the mechanical properties of raw bamboo are unstable [11]. The reliability of the nodes of raw bamboo structures is poor, and it is not suitable to be processed [12, 13]. Therefore, the use of raw bamboo as a structure has great limitations.

The emergence of engineered bamboo makes up for the shortcomings of raw bamboo. Its mechanical properties are stable, and components of various sizes and shapes can be manufactured

Received: 24 November 2024; Received in revised form: 4 February 2025; Accepted: 8 February 2025

according to the needs, which are widely used in construction [14-20]. There are three common types of engineered bamboo: laminated bamboo lumber (LBL) [21-28], glued bamboo [29-32], and Parallel Bamboo Strand Lumber (PBSL) [33]-[35]. The strength and rigidity of laminated bamboo is equivalent to that of wood [36, 37], and it is very suitable for beams and columns. Notable examples (**Fig. 1**) of LBL structures designed by Haitao Li's team have been built recent years, such as Ganzhou Sentai Bamboo R&D Center Building [38], Wuyi 'Bamboo Cubic' Ecological Science and Technology Museum [39], Coconut Post of *Boao Forum for Asia*, and Engineered bamboo bridge structure in Nanjing Forestry University [40]. However, LBL still has many shortcomings as a bending test piece [41-43]. There are also some scholars [44, 45] who have studied the bending resistance of LBL beams, and the results show that the failure mode of the beam is the failure in the tension zone, and the compression zone is better. Therefore, this paper takes the full use of the compression zone of the beam as the starting point to carry out the research.

(a) Sentai Bamboo R&D Center Building in Jiangxi, China [38]

(b) Bamboo Cubic in Fujian, China [39]

(c) Coconut Post in Hainan, China

(d) Engineered bamboo bridge structure in Nanjing, China [40]

Fig. 1 LBL construction projects

FRP is widely used to reinforce LBL due to its advantages such as high strength, corrosion resistance, light weight, and simple construction [46-49]. De Lorenzis et al. [50] conducted test with built-in reinforcement on T-shaped and rectangular reinforced concrete beams using FRP material types, reinforcement ratios and other parameters, and the results showed that most of the failure modes of the beams were bond failure followed by peeling failure. Its excellent performance has not been better played. Taljsten et al. [51] discussed the influence of the bond anchorage length on the flexural capacity by embedding CFRP square bars in the surface of a rectangular reinforced concrete beam. The test showed that for the same reinforcement of CFRP bars, the longer the anchoring length, the more the flexural bearing capacity of the test beam increases. Wang et al. [52] proved that wrapping Aramid Fiber Reinforced Polymer (AFRP) around LBL columns can improve the compressive bearing capacity. Micelli et al. [53] used embedded CFRP bars to repair worn-out glulam beams and studied the performance of their joints. The results show that the CFRP bars are effective and the greater the embedding depth of the CFRP tendons, the more obvious the repair effect. Vahedian et al. [54] applied FRP to the surface of glulam beams, and the experimental results showed that the stiffness of glued beams increased with the increase of the number of bonding layers of FRP.

The method of applying prestressing in the LBL beam has gradually gained acceptance. Wei et al. [55] conducted a test of embedded prestressed steel bars in LBL beams. The test results show that the flexural stiffness of the beam increases with the increase of the reinforcement ratio, and can be increased by up to 36.80%. Prestressing methods in bamboo glulam beams have been shown to be effective [56]-[58]. De Luca et al. [59] proved through experimental studies that prestressed reinforcement can enhance the strength, stiffness and bearing capacity of glulam timbers. Yang et al. [60] used CFRP bars

to strengthen the prestressed glulam beams, and the results showed that the flexural bearing capacity of the reinforced beams increase by 131%, and the flexural rigidity increase by 42.0%.

Although there is more and more research by experts on LBL beams, the research on the application of prestressing in LBL beams is still limited. The FRP bar itself has the characteristics of light weight and high strength. The author considered the operability and economy of the test and proposed a reinforcement method for embedding prestressed bars on the bottom of the LBL beam, and studied the mechanical properties of prestressed GFRP bars on the LBL beam. The influential factors include the reinforcement ratio and the level of the prestress. A formula for calculating the flexural bearing capacity of LBL beams is proposed. Finally, FEM was included to simulate the performance of LBL beams, aimed to reveal the failure pattern and strengthening mechanism.

2 Test materials

A paper for publication can be subdivided into multiple sections: title, list of all the authors and their affiliations, a concise abstract, keywords, main text (including figures, equations, and tables), acknowledgement, references, and appendix.

The LBL beams used in this article are produced by Guangxi Lvjing Bamboo Industry Co., Ltd. The pressing method is hot pressing, which means the raw bamboo is processed into slender bamboo pieces of 2005 mm × 21 mm × 7 mm and pressed at a pressure of 9 MPa for 15 minutes under at 157 degrees Celsius. The dimensions of the test specimens refer to the corresponding standards of ASTM D143 [61]. The basic mechanical properties of the material were tested by the New Sansi universal testing machine. The cross-sectional size of the compression specimens is 50mm×50mm, and the height is 150mm. The size of the tensile specimens is 21 mm × 5 mm × 453 mm, and the effective length is 63 mm. The basic tensile and compressive performance tests of LBL were carried out according to Standards for Test Methods of Wood Structures [62]. The basic mechanical properties of the material are listed in **Table 1**.

Table 1 Basic mechanical properties parameters of LBL

	Ultimate load (kN)	Strength (MPa)	Ultimate strain	Elastic modulus (MPa)
Compression test	125.45	49.13	25864.91	8108
Tensile test	10.09	95.19	13700.46	7444

The compressive strength and elastic modulus of LBL specimens are calculated according to Eq. (1) and Eq. (2) [63]:

$$f_c = P_{max} / A_c \tag{1}$$

$$E_c = \frac{\Delta F_c}{A_c \Delta \varepsilon_c} \tag{2}$$

Among them, f_c is the compressive strength of the compressive specimen (MPa); P_{max} is the ultimate compressive load of the specimen (kN); A_c is the cross-sectional area of the compression surface of the specimen (mm^2); ΔF_c is the load increment at the elastic stage (kN); $\Delta\varepsilon_c$ is the strain increment under the ΔF_c action; $\Delta\varepsilon_y$ is the vertical strain increment in the elastic stage; $\Delta\varepsilon_x$ is the lateral strain increment in the elastic stage.

The tensile strength and tensile elastic modulus of the specimen can be calculated according to Eq. (3) and Eq. (4):

$$\sigma_t = P_{max} / A \tag{3}$$

$$E_t = \frac{\Delta \sigma_t}{\Delta \varepsilon_t} = \frac{\Delta P_t}{A \Delta \varepsilon_t} \tag{4}$$

where, σ_t is the tensile strength of the specimen (MPa); P_{max} is the ultimate tensile load (kN); A is the cross-sectional area of the tensile specimen (mm^2). ΔP_t is the load increment (kN); $\Delta\varepsilon_t$ is the strain amount of the specimen under the action of the load increment ΔP_t.

The GFRP bars selected for the test were produced by Nan Jing Fiber Composite materials Co., Ltd. The tensile strength of FRP bars can be calculated according to Eq. (5) [64]:

$$f_u = F_u / A_u \tag{5}$$

where, f_u is the tensile strength of the FRP bar (MPa); F_u is the maximum load of the FRP bar in the tensile elastic stage (N); A_u is the cross-sectional area of the FRP bar specimen (mm^2). The specific test results are shown in **Table 2**.

The adhesive used for the test is NJMKT390 modified epoxy resin glue produced by Nanjing Mankate Technology Co., Ltd. The splitting tensile strength is 9.46 MPa, the bending strength is 72.5 MPa, and the compressive strength is 107.7 MPa.

Table 2 Mechanical properties parameters of GFRP bars with different diameters

Diameter (mm)	Cross-sectional area (mm^2)	Ultimate load (kN)	Strength (MPa)
8.39	55.26	46.59	843.1
10.41	85.02	78.49	923.2
12.45	121.7	107.70	885.1

3. Laminated bamboo lumber beams test

3.1 Test Design

In this test, 10 groups of specimens were designed with the prestress level and reinforcement ratio as the influencing factors. Each group of specimens included three LBL beams, and the dimensions of the beams were 2000 mm × 100 mm × 150 mm. In order to investigate the influence of the diameter of the GFRP bars on the bending behavior, GFRP bars with diameters of 8 mm, 10 mm and 12 mm were embedded at the bottom of the LBL beams and assigned the numbers GS08, GS10 and GS12. It is necessary to ensure that the centroid position of the GFRP reinforcement embedded in the beam is the same distance from the bottom surface of the beam, so the slot position of the beam section must be set reasonably. **Fig. 2**. shows the cross-section of various types of LBL beams. A 12 mm GFRP bar was embedded in the LBL beam and a prestress of 15%σ_{sy} was applied, and the number of this type of specimen was GS12I. And the beams numbered GS12II are embedded with 12 mm GFRP bars and a prestress of 5%σ_{sy} is applied. The number and parameters of the beams are shown in **Table 3**.

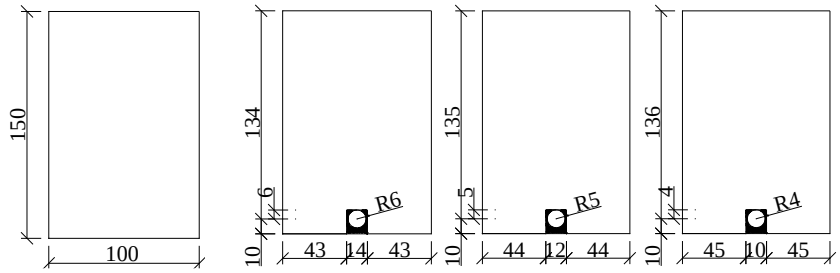

(a) Control beam (b) Beams with 12,10, and 8 mm GFRP bars

Fig. 2 Sectional details of the LBL beams (mm)

The steps of making a prestressed beam are as follows:

(1) Spreading a layer of planting glue evenly in the groove at the bottom of the beam, and put the GFRP bar into the groove at the bottom of the beam. It is required to have threads at both ends and equipped with nuts of suitable size when the GFRP bar is made by the manufacturer.

(2) Pasting the strain gauge at the middle position of the GFRP bar, and install the ordinary displacement gauge at the mid-span position of the beam. After that, the strain gauges and displacement gauges are connected with the TDS data acquisition instrument, and this step is used to monitor the magnitude of the tensile prestress.

(3) Anchoring the GFRP bar at one end through the nut, and continuously tighten the high-strength nut at the other end with a wrench manually during the process of tensioning the GFRP bar. And observing the position of the GFRP bar at all times to prevent the bar body from rotating in the groove. The tensioning can be stopped when it is observed that the strain value displayed on the TDS data acquisition instrument reaches the target control value.

(4) Recording the strain and mid-span displacement data within 48 hours to control the loss of

prestress and replenish the prestress by continuously tightening the nut. The surface is sealed with glue and smoothed after the prestress is stabilized, and maintained for seven days. The fabrication process of the prestressed GFRP bar specimen is shown in **Fig. 3**.

Table 3 Specimen parameters

Group	Number	GFRP bar diameter (mm)	GFRP bar number	Prestress level	Reinforcement ratio (%)
BS0	3	0	0	0	0
GS08	3	8	1	0	0.34
GS08I	3	8	1	$15\%\sigma_{sy}$	0.34
GS08II	3	8	1	$5\%\sigma_{sy}$	0.34
GS10	3	10	1	0	0.53
GS10I	3	10	1	$15\%\sigma_{sy}$	0.53
GS10II	3	10	1	$5\%\sigma_{sy}$	0.53
GS12	3	12	1	0	0.77
GS12I	3	12	1	$15\%\sigma_{sy}$	0.77
GS12II	3	12	1	$5\%\sigma_{sy}$	0.77

(a) Slotting (b) GFRP bar (c) Gluing (d) Prestressing

(e) Monitoring (f) Smoothing (g) Specimens maintenance

Fig. 3 Specimen production

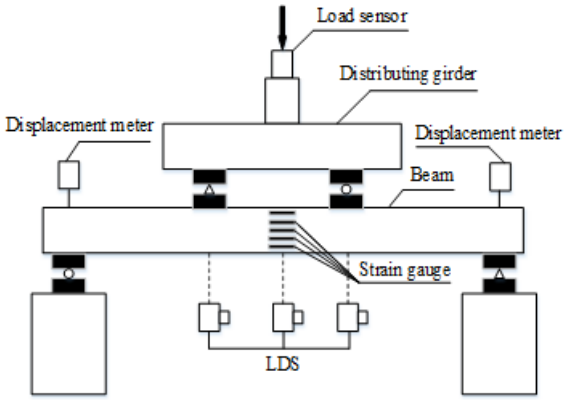

Fig. 4 Text scheme

3.2 Loading scheme

Fig. 4 shows the loading device and arrangement of measuring points during the test. The test is performed under four-point bending load, and the loading scheme follows the method of first force control and then displacement control according to the Standard for Test Methods of Timber Structures [62]. The net span of all simply supported beams is 1800mm, and the load is transferred to the test beam through the distributed beams at two loading points. The side of the beam number is specified as the A side, and the clockwise side is marked as B, C, and D sides. Pasting five strain gauges equidistantly along the height direction on surface A, numbered 2, 3, 4, 5 and 6 respectively. The strain gauge on the B (top) side of the beam numbered 1, and on the D (bottom) side numbered 7. Three laser displacement meters (LDS) are installed at the midspan position at the bottom of the beam and the one-third of the span of the beam. Two displacement meters are installed at both ends of the specimen.

3.3 Failure modes

The failure forms of typical specimens are shown in **Fig. 5** and **Fig. 6**. The first form of failure was the fracture of bamboo fibers in the tension zone of the beam. For description, the typical specimen GS08II-1 is taken as an example. The beam has no significant deformation in the elastic stage. Then, the beam reached the yield point and entered the non-linear stage when the load increased to 58.26 kN and the corresponding displacement was 30.61 mm. When the load increased to 69.85 kN and the corresponding displacement was 38.34 mm, the first crisp sound was generated. The bamboo fibers on the D (bottom) surface broke and produced cracks, which then spread from the mid-span to the loading point and to the A and C surfaces. When the load increased to 74.11 kN and the corresponding displacement was 43.71 mm, the beam bent significantly at this time. Then, the cracks on the A surface continued to extend to the top, and the GFRP bars bent more than the bottom of the beam, and were finally exposed. At the final failure, a series of slender longitudinal cracks formed on the A and C surfaces, penetrating the purely curved section, while the B surface (top surface) was in good condition, and no obvious yield failure occurred. For this beam, the ultimate load was 75.31 kN, and the corresponding displacement was 46.25 mm.

Fig. 5 Fracture of bamboo fiber in the tension zone

Most of the specimens showed this failure mode [41, 43, 65]. The reason for this failure mode is that during the compression process, the LBL at the bottom of the beam reaches the ultimate strength and the specimen fractures. Meanwhile, the GFRP bar is in the elastoplastic stage and the tensile strength is not reached, so the mid-span section at the bottom of the beam breaks. At the same time, the adhesive breaks, and the GFRP bar is exposed without breaking.

The second form was shear failure at the end. The typical sample GS12-I is used as an example for description. In the early stage, the deformation of the beam increases with increasing of the load. The beam suddenly showed huge cracks along the neutral axis when the load increased to 77.13 kN, and the

corresponding displacement was 55.02 mm. At this time, the beam has been completely destroyed, and it is not suitable to continue loading.

Fig. 6 End shear failure

To sum up, the failure modes of control beams, prestressed GFRP reinforced beam and GFRP reinforced beam are similar. In general, the bamboo fibers at the bottom of the beam fractures under tension, and there is no obvious yield failure in the compression zone at the top of the beam. It is preliminarily concluded that the LBL at the top of the beam has been damaged before reaching the ultimate strength and has not been fully utilized. All specimens experienced a sudden brittle fracture failure after undergoing the elastic phase and the elastoplastic phase, but the mid-span deflection during failure was far beyond the $L/250$ value of the specimen's span.

3.4 Test results

The test results of beams are shown in **Table 4**. The average ultimate load of control beams is 58 kN, and the average ultimate displacement is 31 mm. The ultimate load and ultimate displacement of beams with GFRP reinforcement in the body are improved to a certain extent compared with control beams, and the lifting effect increases with the increase of reinforcement ratio. The ultimate bearing capacity and stiffness of the beam can be enhanced by applying prestressing while arranging GFRP bars in the LBL beam, and the enhancement effect is more obvious with the increase of the prestressing level. Among them, the ultimate load can be increased by up to 62.1% compared with ordinary beams. Therefore, it can be considered that the configuration of prestressed tendons in bamboo glulam beams can enhance the flexural performance of the beams. Where P_u is the value of ultimate load, Δ_u is the value of limit displacement, $P_{L/250}$ is the load for a displacement of $L/250$. L is the span of the beam. $EI_{L/250}$ is the value of stiffness. M_t is the value of test bend moment. M_c is the value of calculation bend moment.

Table 4 The comparison results of the average strength

Number	BS0	GS08	GS10	GS12
Strength (MPa)	69.6	85.56	87.6	93.24
Growth Rate (%)		22.9	25.9	34.0
Number	BS0	GS08	GS08II	GS08I
Strength (MPa)	69.6	85.56	86.4	89.64
Growth Rate (%)		22.9	24.1	28.8
Number	BS0	GS08I	GS10I	GS12I
Strength (MPa)	69.6	89.64	104.04	109.56
Growth Rate (%)		28.8	49.5	57.4

Table 4 shows the strength comparison values of different specimens in each group. It can be seen that the GFRP reinforcement in the body can effectively improve the flexural strength of LBL beams compared with control beams, and it increases with the increase of reinforcement ratio. The test results of the three groups of specimens BS0, GS08 and GS08II show that the strength of the beam with 8mm GRFRP reinforcement in the body is increased by 22.9%, and the strength of the beam with 8mm GRFRP reinforcement in the body and prestressing is increased by 28.8%. The results show the effectiveness of prestressing in improving the flexural strength of LBL beams. By comparing the flexural strength results of the beams of GS08I, GS10I and GS12I, it can be seen that the configuration of GFRP bars in the beam and the application of prestressing can greatly improve the flexural strength of the beam, with a maximum increase of 57.4%.

4. Results analysis

4.1 Prestressing analysis

Fig. 7 shows the beam mid-span strain versus time and prestress versus displacement. As shown in **Fig. 7**(a), the prestress is stretched to the specified value in the initial stage, and the prestress decreases slightly in about 5 hours. The prestress decreases the most after 24 hours. At this time, tightening the screws at one end of the beam until the initial prestress value is reached. This method is simple and easy to operate and is suitable for the tension and control of small prestress values in the laboratory and is superior to some existing prestress methods [58, 66, 67].

Fig.7(b) shows the prestress-displacement curves in the middle of the span. The image shows that the prestress can produce a reverse bending displacement at the mid-span of the beam, with the maximum reaching 1/600 of the beam's span. The displacement increases linearly with the increase of the prestress, and the slope remains basically unchanged. This is consistent with the experimental results of Wei [55].

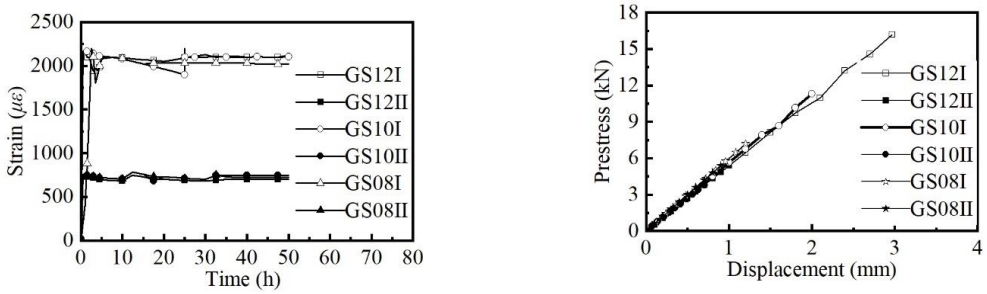

(a) Strain-time curves of prestressed GFRP bars (b) Curves of prestressing-mid-span displacement

Fig. 7 Prestressing process curves

4.1 Load-displacement curves

The load-displacement curves of the control beam and the reinforced-prestressed LBL beams with 8 mm, 10 mm and 12 mm GFRP bars are given in **Fig. 8**. **Fig. 8** (a) shows that the average ultimate loads of BS0 group, GS08I group and GS08II group are 58 kN, 73.7 kN and 72 kN, respectively. With the increase prestressing, the bearing capacity of the beams increased by 27.1% and 24.2%, and the improvement effect was obvious. The average limit displacements of BS0, GS08I and GS08II series specimens were 31 mm, 45.3 mm and 42.7 mm. With the increase of prestress, the ultimate displacement of the specimens increased by 46.1% and 37.7%, respectively.

Fig. 8(b) indicates that the average ultimate load values of BS0 group, GS10I group and GS10II group were 58 kN, 86.7 kN and 79 kN, respectively. With the increase of prestress, the ultimate load of the specimens increased by 49.5% and 36.2%. The average limit displacements of BS0 group, GS10I group and GS10II group were 31 mm, 60 mm and 50.7 mm. With the increasing prestress, the ultimate displacement of the specimen increased by 46.1% and 37.7%.

Fig. 8(c) shows that the average ultimate load values of BS0 group, GS12I group and GS12II group were 58 kN, 91.3 kN and 85.7 kN, respectively. With the increase of prestress, the ultimate load of the specimens increased by 57.4% and 47.8%. The average limit displacements of specimens in BS0 group, GS12I group and GS12II were 31 mm, 70.3 mm and 66.3 mm. The ultimate displacement of the specimen increased by 126.8% and 113.9% the higher the prestress was.

Fig. 8(d) shows that the average value of GS08 series specimens is 71.3 kN, the average value of GS10 series specimens is 73kN and the average value of GS12 specimens is 77.7 kN. The ultimate load of the beams increased by 23%, 25.9%, and 34% with the increase of the reinforcement ratio. Therefore, an appropriate increase in the reinforcement ratio can increase the ultimate bearing capacity of the beam, but this increase is not continuous. When the reinforcement ratio in the beam exceeds a certain value, the enhancement will slow down. For example, the reinforcement ratio of the specimens in the GS08 group is 0.34%, and the ultimate bearing capacity is increased by 23%, and the reinforcement ratio of the specimens in the GS10 group is 0.53%, and the bearing capacity is increased by 25.9%. Excessive

reinforcement ratio may cause over-reinforcement failure of LBL beams, which manifests as shear failure at the beam ends. Therefore, the use of anchors at both ends of the beam can be considered to avoid such situations.

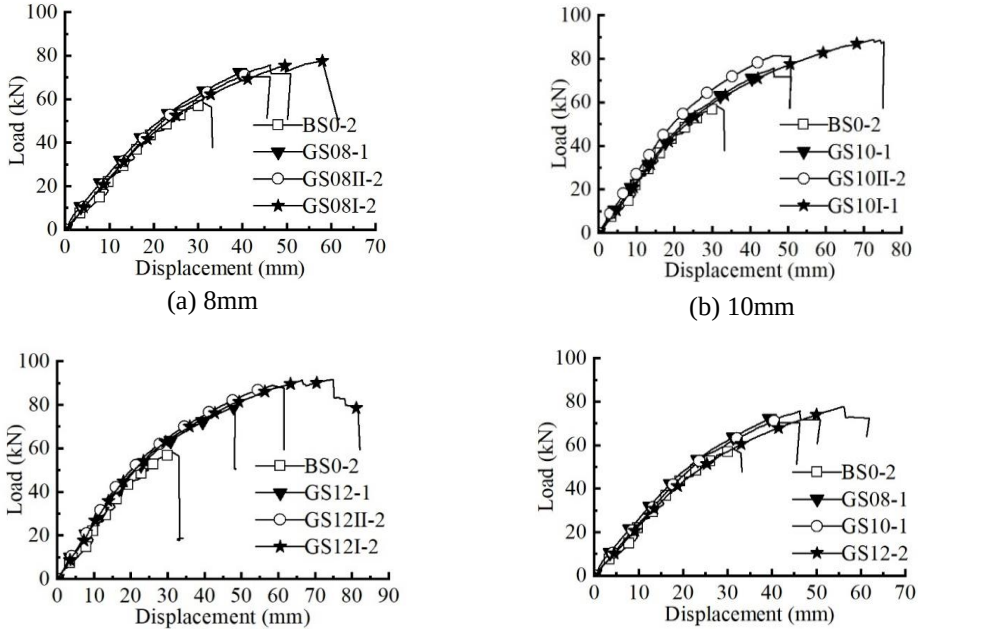

Fig. 8 Load-displacement curves of prestressed GFRP bar beams

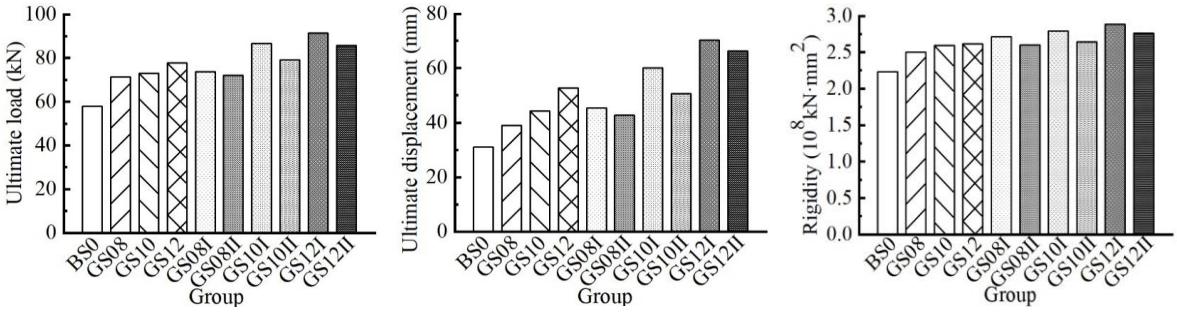

Fig. 9 Comparison of the flexural performance of the LBL beams

In summary, the configuration of prestressed GFRP bars in LBL beams can effectively improve the flexural bearing capacity. Prestress has a positive effect on the ultimate load, ultimate displacement and stiffness of LBL beams. **Fig. 9**. shows the comparison of the flexural performance of the various LBL beams.

4.3 Bending stiffness

The test rigidity of the test piece is measured according to the standard requirements of Wood Structure Test Method Standard, and the *EI* is calculated according to the Eq. (6):

$$EI = \frac{a\Delta P}{48\Delta W}(3L^2 - 4a^2) \tag{6}$$

where, *EI* is the bending stiffness of the member (N·mm^2); a is the distance between the loading point and the supporting point (600 mm). *L* is the calculated span length of the LBL beam (mm), which is 1800mm; ΔP is the load increment (N), and ΔW is the corresponding mid-span deflection increment (mm). Both values are in the elastic stage.

According to the research of scholars [48], the deflection of a wooden beam as a flexural element

in normal service limit state is not more than 1/250 of the beam span. Table 4 summarizes the stiffness of the beam when the displacement is *L*/250 (7.2 mm).

The results show that the stiffness of LBL beams embedded in 8mm, 10 mm and 12 mm prestressed GFRP bars increased by 11.9%, 16.3% and 17.2%. For the prestressed beams of GS08I and GS08II groups, the stiffness increased by 21.6% and 16.7%, respectively. For the prestressed beams of GS10I and GS10II groups, the stiffness increased by 25.1% and 18.5%. For the prestressed beams of GS12I and GS12II groups, the stiffness increased by 29.1% and 23.9%. The effect of prestressing on the stiffness of the specimen is significantly higher than that of the control beam and the beam embedded with GFRP bars of the same diameter. This is because the prestress applied before the test can create a reverse bending deflection, which offsets part of the load and reduces the displacement under the same load during the test.

4.4 Load-strain curves

Fig. 10 shows the load-strain curve of the LBL beams. It can be seen from the figure that the data of the strain gauges on the A and C surfaces have the same trend of change, linearly changing in the early stage, and gradually decreasing due to the compression in the later stage. The data on the B side and the D side are opposite to each other, the B side gradually decreases due to the compression, and the D side becomes larger due to the tension. The ultimate tensile and compressive strain of ordinary beams (BS0) are 6056 $\mu\varepsilon$ and 8628 $\mu\varepsilon$, and the tensile and compressive strain of LBL in Table 1 are compared, and the results show that the former is much lower than the latter. This shows that the materials in the tension zone and the compression zone are not fully functioning when the ordinary beam is damaged.

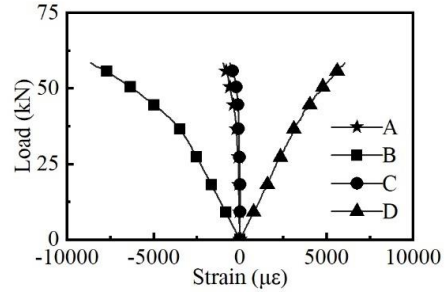

(a) BS0-2

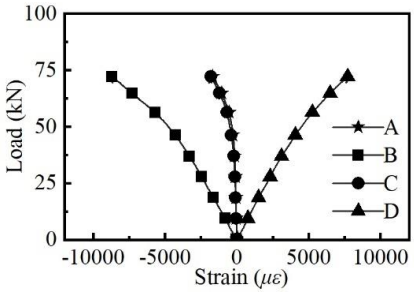

(b) GS08-1

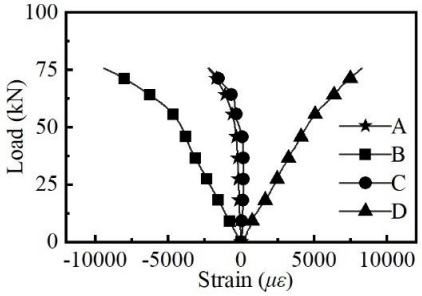

(c) GS10-1

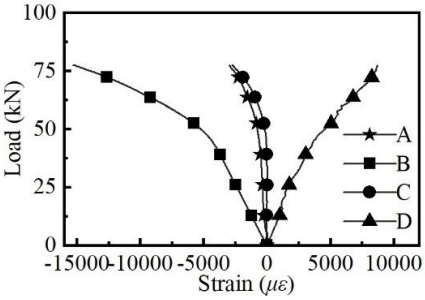

(d) GS12-1

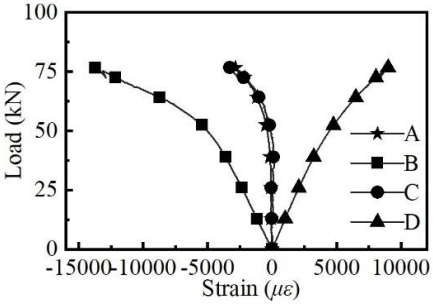

(e) GS081-1

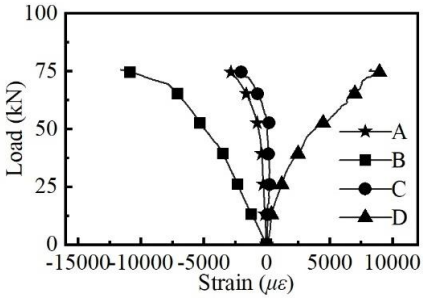

(f) GS082-1

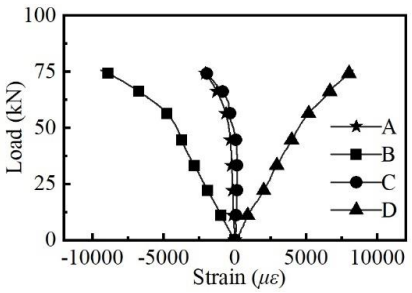

(g) GS101-1

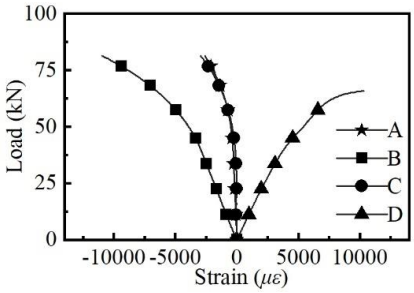

(h) GS102-1

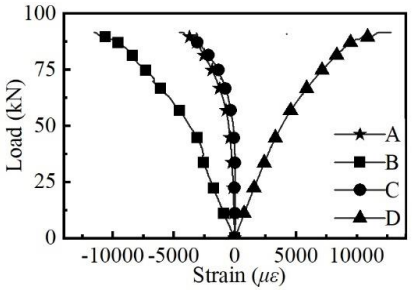

(j) GS121-2

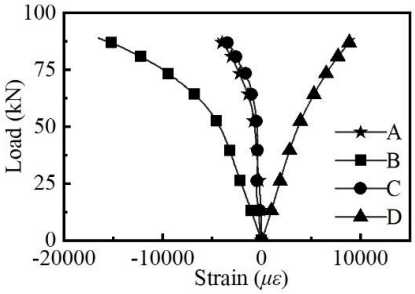

(k) GS122-3

Fig. 10 Load-strain curves

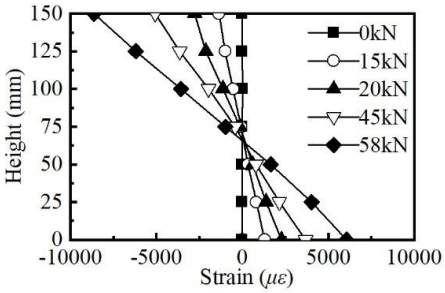

(a) BS0-2

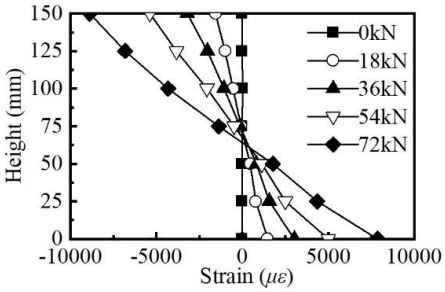

(b) GS08-1

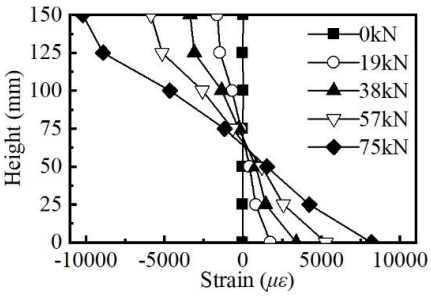

(c) GS10-1

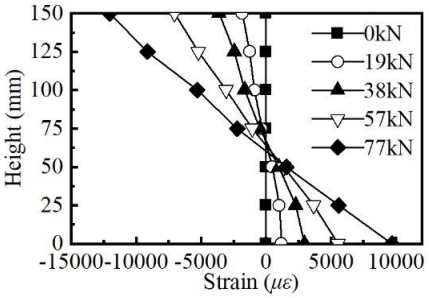

(d) GS12-1

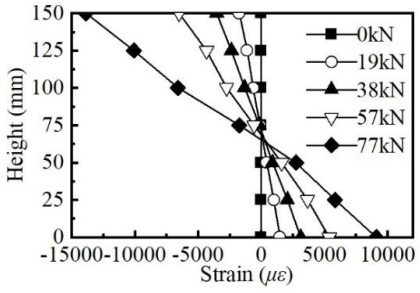

(e) GS081-1

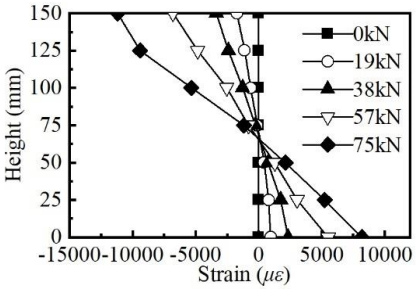

(f) GS082-1

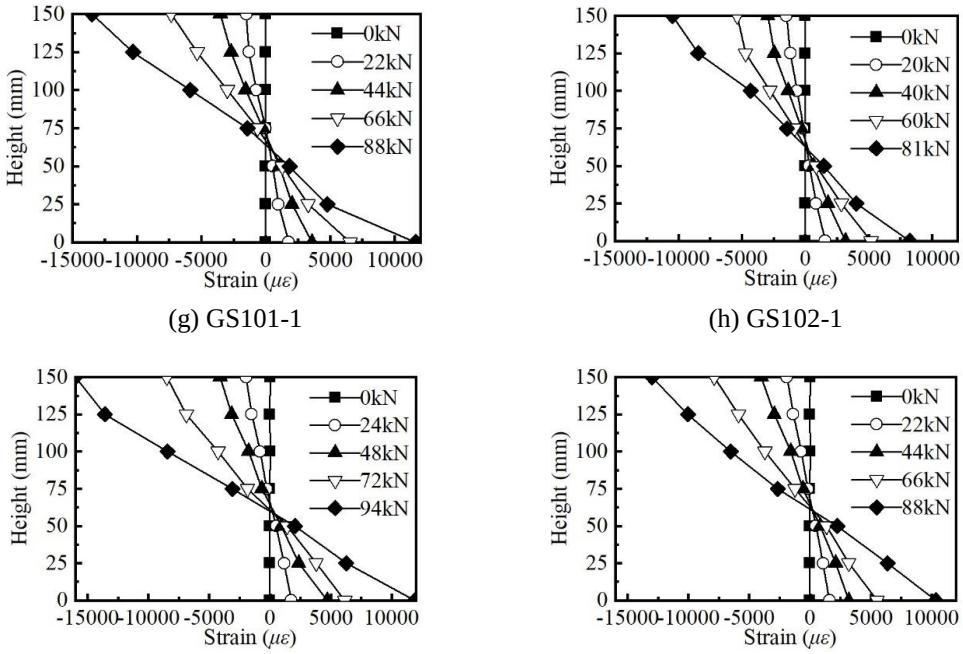

(g) GS101-1 (h) GS102-1

(j) GS121-2 (k) GS122-3

Fig. 11 Strain distribution

The average range of ultimate compressive strain for reinforced beams and prestressed GFRP reinforced beams is12085.4 $\mu\varepsilon$ ~ 13785.3 $\mu\varepsilon$, which is larger than that of ordinary beams. The performance of LBL in the compression zone has been improved by the effect of GFRP bars. The average range of ultimate tensile strain is 12085.4 $\mu\varepsilon$ ~ 13785.3 $\mu\varepsilon$, and the ultimate tensile strain of the prestressed beam with 15% applied is basically the same as that of the LBL material. This shows that the material in the tension zone of the LBL beam with 15% prestress is fully utilized and the failure mode manifests as fracture in the mid-span section at the bottom of the beam.

4.5 Strain distribution

The strain changes of the mid-span section of each group of typical specimens along the section height are shown in **Fig. 11**. The position corresponding to the strain of the mid-span section of the test piece is divided according to the position of the strain gauge. It is stipulated that the height of the corresponding section of the strain gauge at the bottom of the beam is 0 mm and the height of the corresponding section of the strain gauge on the top of the beam is 150 mm. The values of (a) to (k) correspond respectively to a typical specimen of 10 groups of specimens.

For the control beam (BS0-2), the strain of the mid-span section of the specimen shows a linear relationship with the increase of the load, which is in full compliance with the assumption of flat section. The smaller range indicates that the position of the neutral axis does not change significantly between the elastic state and the limit state. For reinforced beam (GS12-1) and prestressed reinforced beam (GS12II-3), the strain increases linearly at the beginning of loading, but in the later loading stage, the strain increases nonlinearly due to the presence of FRP bars, which is basically in line with the assumption of flat section. It can be clearly seen in the figure that the neutral axis moves downward (tension zone) when the ultimate load of the beam is reached.

For the control beam (BS0), the position of the neutral axis is 70.1mm. For the reinforced beams of the groups GS08, GS10 and GS12, the position of the neutral axis is 68.0 mm, 65.1 mm and 62.3 mm. For the prestressed reinforced beams of the groups GS08I, GS10I and GS12I, the position of the neutral axis is 67.8 mm, 66.0 mm and 57.8 mm, respectively. Since the configuration of GFRP bars in the tension zone can increase the moment of inertia of the beam cross-section, and it causes the neutral axis position of the LBL beam to move downward. The larger the prestress, the more obvious the downward.

5. Theoretical analysis

Based on the tensile-compression stress-strain relationship of LBL, this paper deduces the flexural bearing capacity of prestressed LBL beam and gives a general formula for the calculation of bearing capacity combined with previous studies. The calculations are based on the following assumptions:

(1) The material is uniform, ignoring the original defects of the material.

(2) There is no relative slip between the glulam and the GFRP bars.

(3) Before the specimen fails, the strain is linearly distributed along the height of the section, which conforms to the assumption of a flat cross-section.

(4) The theoretical calculation is based on the basic mechanical model of LBL. (The stress-strain calculation model is based on the method proposed by Li [44] as shown in **Fig. 12**.

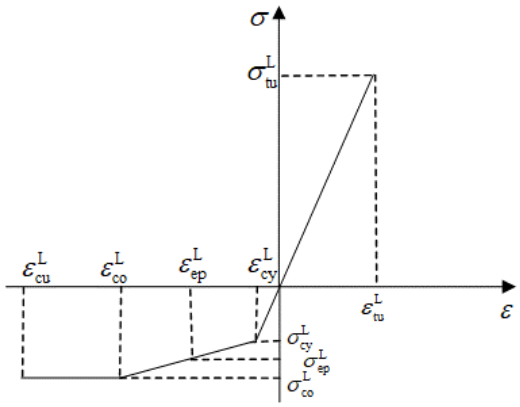

Fig. 12 Stress-strain curve of laminated bamboo lumber [44]

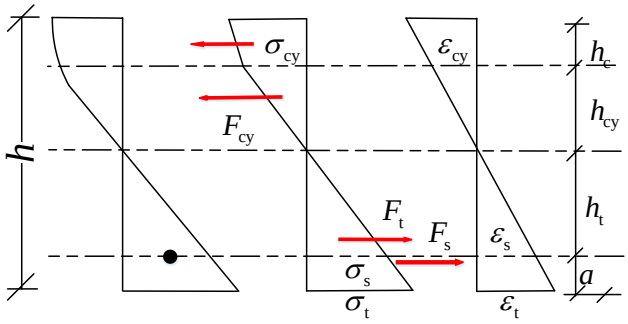

Fig. 13 Stress and strain distribution diagram of LBL at limit state

The model can be expressed by Eq. (7), (8):

$$\sigma=\begin{cases}E_{\mathrm{t}}^{\mathrm{L}}\varepsilon & \left(0\le\varepsilon\le\varepsilon_{\mathrm{tu}}^{\mathrm{L}}\right)\\ E_{\mathrm{c}}^{\mathrm{L}}\varepsilon & \left(\varepsilon_{\mathrm{cy}}^{\mathrm{L}}\le\varepsilon\le 0\right)\\ \sigma_{\mathrm{cy}}^{\mathrm{L}}+k_{\mathrm{ep}}^{\mathrm{L}}E_{\mathrm{c}}^{\mathrm{L}}\left(\varepsilon-\varepsilon_{\mathrm{cy}}^{\mathrm{L}}\right) & \left(\varepsilon_{\mathrm{co}}^{\mathrm{L}}\le\varepsilon\le\varepsilon_{\mathrm{cy}}^{\mathrm{L}}\right)\\ \sigma_{\mathrm{co}}^{\mathrm{L}} & \left(\varepsilon_{\mathrm{cu}}^{\mathrm{L}}\le\varepsilon\le\varepsilon_{\mathrm{co}}^{\mathrm{L}}\right)\end{cases} \tag{7}$$

$$k_{\mathrm{ep}}^{\mathrm{L}}=\frac{\sigma_{\mathrm{co}}^{\mathrm{L}}-\sigma_{\mathrm{cy}}^{\mathrm{L}}}{E_{\mathrm{c}}^{\mathrm{L}}\left(\varepsilon_{\mathrm{co}}^{\mathrm{L}}-\varepsilon_{\mathrm{cy}}^{\mathrm{L}}\right)}=\frac{\sigma_{\mathrm{ep}}^{\mathrm{L}}-\sigma_{\mathrm{cy}}^{\mathrm{L}}}{E_{\mathrm{c}}^{\mathrm{L}}\left(\varepsilon_{\mathrm{ep}}^{\mathrm{L}}-\varepsilon_{\mathrm{cy}}^{\mathrm{L}}\right)} \tag{8}$$

where σ is the value of stress, $E_{\mathrm{t}}^{\mathrm{L}}$ and $E_{\mathrm{c}}^{\mathrm{L}}$ are the elastic modulus of the LBL along the grain under tension and compression, respectively, ε is the value of strain , $\sigma_{\mathrm{cy}}^{\mathrm{L}}$ and $\varepsilon_{\mathrm{cy}}^{\mathrm{L}}$ are the stress and strain of the proportional ultimate compression, $\varepsilon_{\mathrm{tu}}^{\mathrm{L}}$ and $\varepsilon_{\mathrm{cu}}^{\mathrm{L}}$ are the ultimate tensile strain and ultimate compressive strain of the LBL, $\sigma_{\mathrm{co}}^{\mathrm{L}}$ and $\varepsilon_{\mathrm{co}}^{\mathrm{L}}$ are the stress and strain corresponding to the peak compressive load, $\sigma_{\mathrm{ep}}^{\mathrm{L}}$ and $\varepsilon_{\mathrm{ep}}^{\mathrm{L}}$ are the stress and strain values in the elastoplastic stage. $k_{\mathrm{ep}}^{\mathrm{L}}$ is the reduction factor of the modulus in the elastoplastic stage. $\varepsilon_{\mathrm{cy}}^{\mathrm{L}}$ and $\varepsilon_{\mathrm{co}}^{\mathrm{L}}$ are 4625 $\mu\varepsilon$ and 25864 $\mu\varepsilon$, $E_{\mathrm{t}}^{\mathrm{L}}$ and $E_{\mathrm{c}}^{\mathrm{L}}$ are 7444 MPa and 8108 MPa.

The stress σ_{ep} in the compression zone is between σ_{cy} and σ_{co} combined with the results in Table 1, and the stress and strain distribution of GFRP bars reinforced LBL beam is shown in **Fig. 13**.

In **Fig. 13**, h is the height of the beam (100 mm), h_{c} and h_{cy} are the heights of the compression zone of the LBL beam, and h_{t} is the height of the tension zone. a is the distance from the center of the GFRP bar to the bottom of the beam (10 mm).

Combining **Fig. 13** with Eq. (7) and Eq. (8) to find the stress value at each stage:

$$\sigma_{\mathrm{cy}}=E_{\mathrm{c}}\varepsilon \tag{9}$$

$$\sigma_{\mathrm{c}}=\sigma_{\mathrm{cy}}+k_{\mathrm{ep}}E_{\mathrm{c}}\left(\varepsilon-\varepsilon_{\mathrm{cy}}\right)=E_{\mathrm{c}}\varepsilon+k_{\mathrm{ep}}E_{\mathrm{c}}\left(\varepsilon-\varepsilon_{\mathrm{cy}}\right) \tag{10}$$

$$\sigma_{\mathrm{t}}=E_{\mathrm{t}}\varepsilon \tag{11}$$

$$\sigma_s = \frac{h_t - a}{h_t}\sigma_t + \sigma_p = \frac{h_t - a}{h_t}E_s\varepsilon_t + E_s\varepsilon_p \tag{12}$$

where, σ_{cy} and ε_{cy} are the ultimate stress value and strain value of the compression zone in the elastic stage, respectively, σ_c is the ultimate stress value of the compression zone in the elastoplastic stage, σ_t and ε_t are the ultimate stress values in the tension zone, σ_s is the stress value of the GFRP bar in the tension zone, E_s is the elastic modulus of the GFRP bar, σ_p and ε_p are the stress and strain values of the prestressed GFRP bar.

Eq. (13) results from the equilibrium of forces:

$$F_c + F_{cy} = F_t + F_s \tag{13}$$

where, F_c is the resultant force of the plastic compression zone, F_{cy} is the resultant force of the elastic compression zone, F_t is the force of the tension zone, F_s is the resultant force of the GFRP bar, A_s is the cross-sectional area of the GFRP bar.

The four resultant forces can be obtained by Eq. (14), Eq. (15), Eq. (16) and Eq. (17):

$$F_c = \left(\sigma_{cy} + \sigma_c\right)h_c b / 2 \tag{14}$$

$$F_{cy} = \sigma_{cy}h_{cy}b / 2 \tag{15}$$

$$F_t = \sigma_t h_t b / 2 \tag{16}$$

$$F_s = \sigma_s A_s \tag{17}$$

According to the geometric relationship in **Fig. 13**, Eq. (18) is obtained:

$$h_{cy} = \varepsilon_{cy}h_t / \varepsilon_t \tag{18}$$

Let $\varepsilon_{cy} / \varepsilon_t = N$ .According to the tensile and compressive tests of the LBL, with $\varepsilon_{cy} = 0.0046$, $\varepsilon_t = 0.0137$, N = 0.34.

$$h_c = h - \left(N + 1\right)h_t \tag{19}$$

Combining Eq. (17) and (18), it can be concluded that the neutral axis height can be expressed by Eq. (19) when the cross section is in the ultimate state:

$$h_t = \frac{-B \pm \sqrt{B^2 - 4AC}}{2A} \tag{20}$$

with:

$$A = bE_c\left\{\left[\left(2 + k_{ep}\right)\varepsilon - k_{ep}\varepsilon_{cy}\right]\left[h - \left(N + 1\right) + \varepsilon N\right]\right\} - E_t\varepsilon \tag{21}$$

$$B = -2\left(E_t\varepsilon + E_s\varepsilon_p\right) \tag{22}$$

$$C = 2aE_t\varepsilon \tag{23}$$

According to the Equations given above, the calculation value (M_c) of bending moment can be obtained:

$$M_c = F_c \bullet \left(h - h_t - \frac{h_c}{3}\frac{2\sigma_{cy} + \sigma_c}{\sigma_{cy} + \sigma_c}\right) + F_{cy}\frac{2}{3}h_c + F_t\frac{2}{3}h_t + F_s\left(h_t - a\right) \tag{24}$$

The test value of the bending moment can be expressed by Eq. (25):

$$M_t = PL / 6 \tag{25}$$

where, P is the external load and L is the net span of the beam.

Table 5 shows the comparison between the test bending moment value and the calculated bending moment value. It can be seen that the test value of the specimens agrees well with the calculation value except for GS08 I -2, GS08II-1 and GS10II-2. The average error of the test piece is 4.61%. For the three

GS12I series beams, the average error is only 1.2%, which basically agrees with the experimental value. The results show that the section stress analysis model established in this way can be used for the calculation of the bearing capacity of the beam.

Table 5 Test results

Group	P_u (kN)	Increase ratio of P_u	Δ_u (mm)	$P_{L/250}$ (kN)	$EI_{L/250}$ (10^8kN·m^2)	Increase ratio of $EI_{L/250}$	M_t (kN·m)	M_c (kN·m)	Error (%)
BS0-1	60	-	32	18.96	2.45	-	18	16.68	-7.33
BS0-2	58	-	31	14.92	1.93	-	17.4	16.89	-2.93
BS0-3	56	-	30	17.87	2.31	-	16.8	15.65	-6.84
Average	58	-	31	17.25	2.23	-	17.4	16.41	-5.7
GS08-1	72	24.1	38	17.82	2.31	3.3	21.6	22.36	3.52
GS08-2	73	25.9	39	20.54	2.66	19.1	21.9	22.48	2.65
GS08-3	69	19.0	40	19.52	2.53	13.2	20.7	21.56	4.15
Average	71.3	22.9	39	19.3	2.5	11.9	21.39	22.13	3.44
GS10-1	75	29.3	47	21.32	2.76	23.6	22.5	24.55	9.11
GS10-2	68	17.2	42	17.25	2.23	0	20.4	22.39	9.75
GS10-3	76	31.0	44	21.59	2.79	25.2	22.8	24.64	8.07
Average	73	25.9	44.3	20.05	2.59	16.3	21.8	23.86	8.07
GS12-1	77	32.8	55	19.29	2.5	11.8	23.1	24.56	6.32
GS12-2	77	32.8	55	20.18	2.61	17.0	23.1	24.69	6.88
GS12-3	79	36.2	48	21.16	2.74	22.7	23.7	24.82	4.72
Average	77.7	34.0	52.7	20.21	2.61	17.2	23.31	24.69	5.97
GS08I-1	77	32.8	58	19.76	2.56	14.6	23.1	24.65	6.71
GS08I-2	76	31.0	56	19.14	2.48	11.0	22.8	25.12	10.17
GS08I-3	71	22.4	38	23.99	3.10	39.1	21.3	23.43	10
Average	74.7	28.8	50.7	20.96	2.71	21.6	22.41	24.4	8.96
GS08II-1	75	29.3	46	23.49	3.04	36.2	22.5	25.12	11.64
GS08II-2	72	24.1	39	18.46	2.39	7.1	21.6	22.90	6.02
GS08II-3	69	19.0	43	18.41	2.38	6.8	20.7	20.45	-1.21
Average	72	24.1	42.7	20.12	2.6	16.7	21.6	22.82	6.29
GS10I-1	88	51.7	61	21.47	2.78	24.5	26.4	27.65	4.73
GS10I-2	86	48.3	55	21.32	2.76	23.6	25.8	27.23	5.54
GS10I-3	86	48.3	64	21.94	2.84	27.2	25.8	27.75	7.56
Average	86.7	49.5	60	21.58	2.79	25.1	26.01	27.54	5.94
GS10II-1	81	39.7	46	22.10	2.86	28.2	24.3	26.31	8.27
GS10II-2	79	36.2	48	19.6	2.54	13.6	23.7	26.38	11.31
GS10II-3	77	32.8	58	19.6	2.54	13.6	23.1	25.62	10.9
Average	79	36.2	50.7	20.43	2.64	18.5	23.7	26.10	10.16
GS12I-1	94	62.1	62	25.72	3.33	49.1	28.2	27.92	-0.99
GS12I-2	91	56.9	75	20.68	2.68	19.9	27.3	28.13	3.04
GS12I-3	89	53.4	74	20.37	2.64	18.1	26.7	27.12	1.57
Average	91.3	57.4	70.3	22.26	2.88	29.1	27.39	27.72	1.21
GS12II-1	84	44.8	52	23.04	2.98	33.6	25.2	24.36	-3.33
GS12II-2	85	46.6	73	19.75	2.56	14.5	25.5	26.85	5.29
GS12II-3	88	51.7	74	21.31	2.76	23.6	26.4	27.24	3.18
Average	85.7	47.8	66.3	21.37	2.76	23.9	25.71	26.15	3.93

6. Finite element modelling

6.1 Material failure criteria

In this paper, LBL was considered as an orthotropic material, as shown in **Fig. 14**, in which direction 1 is along the bamboo fiber direction, direction 2 and 3 are perpendicular to the fiber direction. According to the test results, the failure of LBL beams was main the fracture failure in the tension zone, it included the tension failure of the bamboo fiber, tension splitting failure between bamboo fibers. Thus, in FEM, only the tension failure was considered.

For tension along the fiber direction (direction 1), a maximum stress criterion was adopted:

$$F_{t,1}(\sigma)=\sigma_{11}/\ f_{t,1}\geq 1 \tag{26}$$

where, σ_{11} is the stress in direction 1; $f_{t,1}$ is the tensile strength in direction 1.

For tension splitting failure, a quadratic criterion was used:

$$F_{t,i}(\sigma)=\frac{\sigma_{ii}^2}{f_{t,i}}+\frac{\sigma_{1i}^2}{f_v}+\frac{\sigma_{23}^2}{f_{roll}}\geq 1,\quad \text{i=2 or 3} \tag{27}$$

where, σ_{ii} is the stress in direction i; σ_{1i} is the shear stress in plane 1i; σ_{23} is the shear stress in plane 23; $f_{t,i}$ is the tensile strength in direction i; f_v is the longitudinal shear strength, f_{roll} is the rolling shear strength.

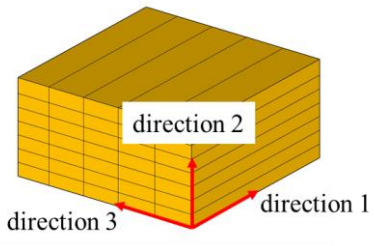

Fig. 14 Material direction of LBL

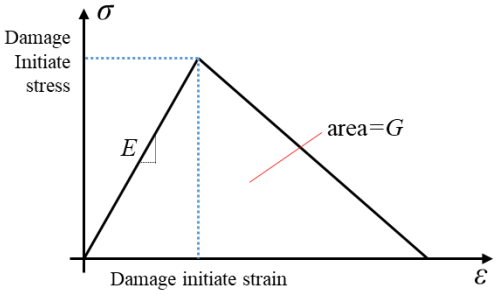

Fig. 15 Damage evolution law

6.2 Damage evolution

When the failure criteria in Eq.(26) and Eq.(27) was satisfied, the damage was triggered. Since both tension failure of bamboo parallel and perpendicular to the fiber direction of LBL were brittle failure, the damage parameter d_i was calculated by a linear softening stress–strain relationship [69] as shown in **Fig. 15**.

$$d_i=1-\frac{1}{f_{t,i}^2-\frac{2G_{f,i}E_i}{L_c}}\left(f_{t,i}^2-\frac{2G_{f,i}E_i}{L_cF_{t,i}(\sigma)}\right),\quad \text{i=1,2,3} \tag{28}$$

where, $G_{f,i}$ is the tensile fracture energy in direction i; E_i is the elastic modulus in direction i; L_c is the characteristic length of the element.

The initial value of d_i was set as 0, when the damage was triggered, d_i started to growing, it then lead to a degradation of the material stiffness matrix, the initial stiffness or the elastic modulus $E_{0,i}$ was changed to $E_{0,i}(1-d_i)$. The maximum value of d_i was set as 0.99 in this paper.

6.3 Modelling information

Based on the mentioned damage initiation and evolution laws, a user defined material subroutine for LBL was developed and adopt in ABAQUS/Explicit. The detailed mechanical parameters of LBL, steel support, and GFRP are shown in **Table 6**. According to Wang et al. [70], the tensile strength of bamboo node is significantly lower than other bamboo areas, thus, to simulate the crack pattern of LBL beams, several areas were selected randomly to apply lower tensile strength at the bottom of the LBL beams to initiate the damage, as shown in **Fig. 16**(a), and element deletion was implemented. C3D8R solid elements were used for both LBL [71] and steel, the meshing details are shown in **Fig. 16**(b). GFRP was simulated by truss element (T3D2), and treated as an embedded region to reinforce LBL beams. To apply prestress of GFRP bars, a cooling down method was used according to the followed equation [72]:

$$T=-\frac{P}{c\cdot E\cdot A} \tag{29}$$

where, T is the aimed temperature, P is the required prestressed force; c is the thermal expansion coefficient of GFRP; E is elastic modulus of GFRP; A is the cross-section area of GFRP bar.

The contact between LBL beam and supports was a general contact, with tangential behavior was coulomb friction model with a friction coefficient of 0.3, and normal behavior was hard contact.

Table 6 Mechanical parameters in FEM

Materials	Elastic modulus (MPa)		Poisson's ratio		Yield strength (MPa)		Fracture energy (N/mm)		Thermal expansion coefficient ($^oC^{-1}$)	
LBL	E_{11}	7500	$\mu_{12} = \mu_{13}$	0.35	$\bar{\sigma}_{11} / \bar{\sigma}_{11,weak}$	60/30	$G_{f,1}$	100		
	$E_{22} = E_{33}$	1600	μ_{23}	0.2	$\bar{\sigma}_{22} = \bar{\sigma}_{33}$	25	$G_{f,2}$=$G_{f,3}$	20		
	$G_{12} = G_{13}$	1300			$\bar{\sigma}_{12} = \bar{\sigma}_{13}$	15				
	G_{23}	100			$\bar{\sigma}_{23}$	5				
GFRP	E	54000	μ	0.3	σ	960			c	5×10^{-6}
Steel support	E	210000	μ	0.3						

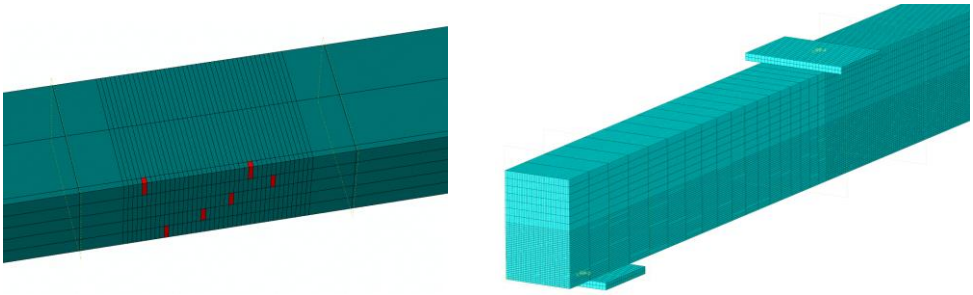

(a) Lower tensile strength area in color red (b) Meshing of LBL beam

Fig. 16 FEM details

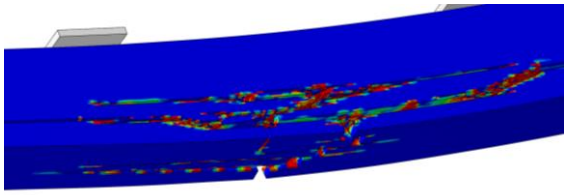

(a) Failure overview

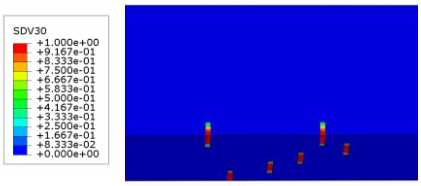

(b) Initial tension damage in direction 1

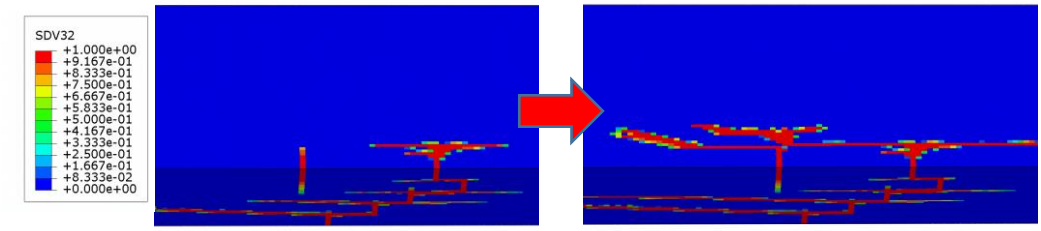

(c) Damage evolution in direction 2

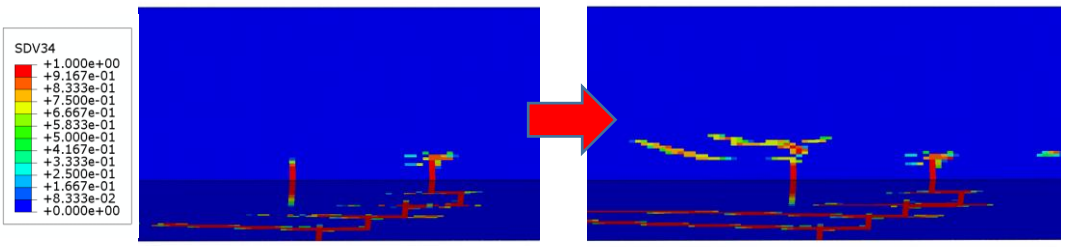

(d) Damage evolution in direction 3

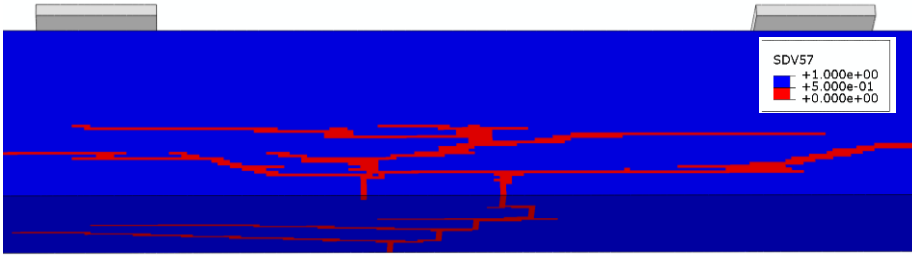

(e) Final element deletion

Fig.17 Failure phenomenon of FEM

6.4 FEM results

The general failure of LBL beams is shown in **Fig. 17**(a), for both normal beams and reinforced beams, the failure pattern were all similar. Tension damage in direction 1 was first generated at the bottom of the beam where weaker tension strength was applied, **Fig. 17**(b). Then with the inconsistent deformation of the damaged and undamaged area, the tension damages in direction 2 and 3 were initiated, and finally led to horizontal cracks on beam's side and bottom planes, **Fig. 17**(c, d). With the increase of the displacement, the tension damage in direction 1 gradually developing from the bottom of the beam upwards, resulted in more horizontal cracks, **Fig. 17**(e).

The load-displacement curves of LBL beams from FEM are shown in **Fig .18**. The same to the experimental results, the use of GFRP bar could obviously enhance the bearing capacity, ultimate displacement, and bending stiffness of LBL beams, **Fig. 18**(a). The increasing ratio of these bending properties were largest from normal LBL beam to a beam strengthened with 8 mm diameter GFRP bars (ultimate load from 73 kN to 80 kN). While with increasing bar diameter (8mm, 10mm, 12mm), the ultimate load increments were only around 2.5 kN. The ultimate displacement and bending stiffness also presented the same pattern.

For the LBL beams with pre-stressed GFRP bars, taking diameter of 10 mm as an example, the load-displacement curves are shown in **Fig. 18**(b). The prestressed GFRP bar could increase the load capacity, and the ultimate displacement. It is worth mention that part of the ultimate displacement increase was due to the upward bending of the beam under the application of prestress. The bending stiffness did not show a rise for increasing prestressed load in FEM. This could be explained by in FEM, prestressed load could not increase the elastic modulus of GFRP bar itself, thus the bending stiffness didn't increase.

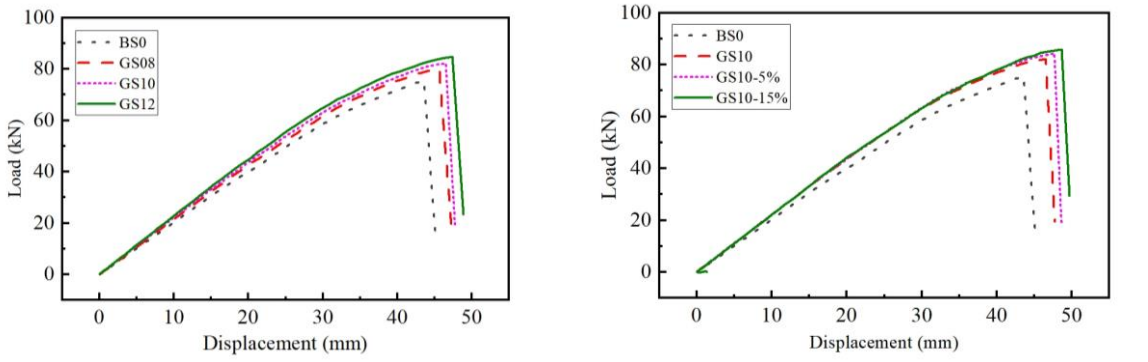

(a) Control beams (b) Prestressed beams

Fig.18 Load-displacement curves of FEM

7. Conclusions

In this paper, the prestress level and reinforcement ratio are the influencing factors to carry out experimental research on LBL beams. The comprehensive analysis draws the following conclusions:

The failure modes of LBL beams are mainly shear failure and bending failure. The strains of the tensile zone and the compression zone of the LBL beam did not reach the ultimate strain of the material

when failure occurred. However, the ultimate strain of the beam can be increased by configuring prestressed GFRP bars at the bottom of the LBL beam, thereby improving the utilization rate of materials. Embedding prestressed GFRP bars in beams can effectively improve the flexural bearing capacity and flexural rigidity of beams compared with control beams. And the bearing capacity and stiffness of the LBL beam increase with the increase of reinforcement ratio and the increase of prestress level. Among them, the flexural bearing capacity of the beam with 12 mm GFRP bars and 15.6 kN prestress applied in the body was increased by 57.4%, and the flexural stiffness was increased by 29.1%. The strengthened beams were simulated by FEM using continuum damage mechanics, the failure pattern and the strengthening mechanism were verified.

The change of section height of ordinary beams and prestressed reinforced beams with strain is in accordance with the principle of flat section assumptions. The position of the neutral axis of the prestressed reinforced beam moves down relative to the control beam, and the greater the prestress, the more the neutral axis of the beam moves downward. According to the stress-strain distribution of the LBL beams when they are flexural damaged, a theoretical formula for calculating the flexural bearing capacity of LBL beams is proposed by combining with the three-stage LBL stress-strain constitutive model. After verification, it is found that the theoretical model is in good agreement with the experimental results.

Acknowledgement

The writers gratefully acknowledge Yukun Tian, Chen Chen, Gensheng Cheng, Han Zhang, Ke Zhou, Xiaoyan Zheng, Shaoyun Zhu, Liqing Liu, Dunben Sun, Jing Cao, Yanjun Liu, Junhong Xu and others from the Nanjing Forestry University for helping.

Funding Statement

This work was supported by the National Natural Science Foundation of China (No. 51878354), the Natural Science Foundation of Jiangsu Province (No. BK20181402), Forestry Science and Technology Innovation and Promotion Project of Jiangsu Province (No. LYKJ[2024]08), 333 talent high-level projects of Jiang-su Province, . Any research results expressed in this paper are those of the writer(s) and do not necessarily reflect the views of the foundations.

CRediT authorship contribution statement

Haitao Li: Conceptualization, Funding acquisition, Supervision, Investigation, Formal analysis, Writing – original draft. **Dong Yang**: Investigation, Formal analysis, Writing – original draft. **Ben Chen**: Investigation, Formal analysis, Writing – original draft. **Sarah Mohrmann**: Writing – review & editing. **Rodolfo Lorenzo**: Supervision, Writing – review & editing. **Kun Zhou**: Writing – review & editing. **Feng Shen**: Writing – review & editing.

Conflicts of Interest

The authors declare that they have no conflicts of interest to this work.

Data Availability Statement

Some or all data, models, or codes that support the findings of this study are available from the corresponding author upon reasonable request.

References

[1] Li X, Ashraf M, Subhani M, Kremer P, Kafle B, Ghabraie K. Experimental and numerical study on bending properties of heterogeneous lamella layups in cross laminated timber using Australian Radiata Pine. Constr Build Mater 2020; 247: 118525. https://doi.org/10.1016/j.conbuildmat.2020.118525.

[2] Dauletbek A, Xue X, Shen X, Li H, et al. Lightweight bamboo structures – Report on 2021 International Collaboration on Bamboo Construction. Sustain Struct, 2023; 3(1): 000025. https://doi.org/10.54113/j.sust.2023.000025.

[3] Liu K, Jayaramana D, Shib Y, et al. “Bamboo: A Very Sustainable Construction Material & the 3rd World

Symposium on Sustainable Bio-Composite Materials and Structures" - 2022 International Conference summary report. Sustain Struct, 2023, 3(2): 000033. https://doi.org/10.54113/j.sust.2023.000033.
[4] Sheng Y, Huang G L, Ye X F, et al. Analysis on mechanical properties of bamboo scrimber under tension stress. J Forest Eng, 2023; 8(1): 46-52. https://doi.org/10.13360/j.issn.2096-1359.202205030.
[5] Ding Y, Zhang Y, Wang Z, Gao Z, Zhang T, Huang X. Vibration test and comfort analysis of environmental and impact excitation for wooden floor structure. BioResources 2020; 15: 8212–34. https://doi.org/10.15376/biores.15.4.8212-8234.
[6] Sun X, He M, Li Z. Novel engineered wood and bamboo composites for structural applications: State-of-art of manufacturing technology and mechanical performance evaluation. Constr Build Mater 2020; 249: 118751. https://doi.org/10.1016/j.conbuildmat.2020.118751.
[7] Mergiaw T, Addissie D, Goedert J. Failure Behavior and Failure Locations of Oxytenanthera Abyssinica Bamboo Culms under Bending Load. Sustain Struct, 2023; 3(2): 000029. https://doi.org/10.54113/j.sust.2023.000029.
[8] Gao Y, Xuan S Q, Meng X M, et al. Research status of timber reciprocal structures. J Forest Eng, 2023; 8(2): 30-39. https://doi.org/10.13360/j.issn.2096-1359.202204037.
[9] Yang H Q, Wu F D, Zhu G Y, et al. Recent progress of modification and industrialization for nanocellulose towards green building materials. J Forest Eng, 2023, 8(3): 11-20. https://doi.org/10.13360/j.issn.2096-1359.202208003.
[10] Sharma B, Gatóo A, Bock M, Ramage M. Engineered bamboo for structural applications. Constr Build Mater 2015; 81: 66–73. https://doi.org/10.1016/j.conbuildmat.2015.01.077.
[11] Hong C, Li H, Lorenzo R, Wu G, Corbi I, Corbi O, et al. Review on connections for original bamboo structures. J Renew Mater 2019; 7: 714–30. https://doi.org/10.32604/jrm.2019.07647.
[12] Pradhan NPN, Paraskeva TS, Dimitrakopoulos EG. Quasi-static reversed cyclic testing of multi-culm bamboo members with steel connectors. J Build Eng 2020; 27: 100983. https://doi.org/10.1016/j.jobe.2019.100983.
[13] Hong C, Li H, Xiong Z, Lorenzo R, Corbi I, Corbi O, et al. Review of connections for engineered bamboo structures. J Build Eng 2020; 30: 101324. https://doi.org/10.1016/j.jobe.2020.101324.
[14] Verma CS, Sharma NK, Chariar VM, Maheshwari S, Hada MK. Comparative study of mechanical properties of bamboo laminae and their laminates with woods and wood based composites. Compos Part B Eng 2014; 60: 523–30. https://doi.org/10.1016/j.compositesb.2013.12.061.
[15] Li Z, Yang GS, Zhou Q, Shan B, Xiao Y. Bending performance of glubam beams made with different processes. Adv Struct Eng 2019; 22: 535–46. https://doi.org/10.1177/1369433218794327.
[16] Chen G, Yu Y, Li X, He B. Mechanical behavior of laminated bamboo lumber for structural application: an experimental investigation. Eur J Wood Wood Prod 2020; 78: 53–63. https://doi.org/10.1007/s00107-019-01486-9.
[17] Qiu Z, Fan H. Nonlinear modeling of bamboo fiber reinforced composite materials. Compos Struct 2020; 238: 111976. https://doi.org/10.1016/j.compstruct.2020.111976.
[18] Mahdavi M, Clouston PL, Arwade SR. A low-technology approach toward fabrication of Laminated Bamboo Lumber. Constr Build Mater 2012; 29: 257–62. https://doi.org/10.1016/j.conbuildmat.2011.10.046.
[19] Li X, Ashraf M, Li H, Zheng X, Wang H, Al-Deen S, et al. An experimental investigation on Parallel Bamboo Strand Lumber specimens under quasi static and impact loading. Constr Build Mater 2019; 228: 116724. https://doi.org/10.1016/j.conbuildmat.2019.116724.
[20] Tan C, Li H, Wei D, Lorenzo R, Yuan C. Mechanical performance of parallel bamboo strand lumber columns under axial compression: Experimental and numerical investigation. Constr Build Mater 2020; 231: 117168. https://doi.org/10.1016/j.conbuildmat.2019.117168.
[21] Verma CS, Chariar VM. Stiffness and strength analysis of four layered laminate bamboo composite at macroscopic scale. Compos Part B Eng 2013; 45: 369–76. https://doi.org/10.1016/j.compositesb.2012.07.048.
[22] Correal JF, Echeverry JS, Ramírez F, Yamín LE. Experimental evaluation of physical and mechanical properties of Glued Laminated Guadua angustifolia Kunth. Constr Build Mater 2014; 73: 105–12. https://doi.org/10.1016/j.conbuildmat.2014.09.056.
[23] Sinha A, Way D, Mlasko S. Structural Performance of Glued Laminated Bamboo Beams. J Struct Eng 2014; 140: 04013021. https://doi.org/10.1061/(asce)st.1943-541x.0000807.
[24] Shan B, Wang G, Lei P, et al. Experimental research on formaldehyde emission characteristics from glubam by climate chamber test. Sustain Struct, 2023; 3(2): 000027. https://doi.org/10.54113/j.sust.2023.000027.
[25] Zhou K, Li HT, Assima D, Yang D, Xiong ZH. Slenderness ratio effect on the eccentric compression performance of chamfered laminated bamboo lumber columns. Journal of Renewable Materials, 2022; 10(1), 165–182. https://doi.org/10.32604/jrm.2021.017223.
[26] Li HT, Liu R, Lorenzo R, Wu G, Wang L Bin. Eccentric compression properties of laminated bamboo columns with different slenderness ratios. Proc Inst Civ Eng Struct Build 2019; 172: 315–326. https://doi.o

rg/10.1680/jstbu.18.00007.
[27] Li HT, Zhang QS, Huang DS, Deeks AJ. Compressive performance of laminated bamboo. Compos Part B Eng 2013; 54: 319–328. https://doi.org/10.1016/j.compositesb.2013.05.035.
[28] Li H, Wu G, Xiong Z, Corbi I, Corbi O, Xiong X, et al. Length and orientation direction effect on static bending properties of laminated Moso bamboo. Eur J Wood Wood Prod 2019; 77: 547–557. https://doi.org/10.1007/s00107-019-01419-6.
[29] Li H, Xu W, Chen C, et al. Temperature Influence on the Bending Performance of Laminated Bamboo Lumber. J Mater Civil Eng, 2023; 35(5): 04023072. https://doi.org/10.1061/(ASCE)MT.1943-5533.0004730.
[30] Y. Xiao, Z. Li, Y. Wu, B. Shan, Research and engineering application progress of laminated bamboo structure, Build Struct 2018; 48 (10): 84-88.
[31] Yu Y, Liu R, Huang Y, Meng F, Yu W. Preparation, physical, mechanical, and interfacial morphological properties of engineered bamboo scrimber. Constr Build Mater 2017; 157: 1032–1039. https://doi.org/10.1016/j.conbuildmat.2017.09.185.
[32] Xiao Y, Yang RZ, Shan B. Production, environmental impact and mechanical properties of glubam. Constr Build Mater 2013; 44: 765–773. https://doi.org/10.1016/j.conbuildmat.2013.03.087.
[33] Zhou K, Li H, Hong C, Ashraf M, Sayed U, Lorenzo R, et al. Mechanical properties of large-scale parallel bamboo strand lumber under local compression. Constr Build Mater 2020; 271: 121572. https://doi.org/10.1016/j.conbuildmat.2020.121572.
[34] Zhong Y, Ren H, Jiang Z. Effects of Temperature on the Compressive Strength Parallel to the Grain of Bamboo Scrimbe 2016; 9(6): 436. https://doi.org/10.3390/ma9060436.
[35] Chen F M, He Y Y, Wei X, et al. Advances in strength and toughness of hierarchical bamboo under humidity and heat. J Forest Eng, 2023, 8(4): 10-18. https://doi.org/10.13360/j.issn.2096-1359.202207008.
[36] Corradi M, Speranzini E, Borri A, Vignoli A. In-plane shear reinforcement of wood beam floors with FRP. Compos Part B Eng 2006; 37: 310–319. https://doi.org/10.1016/j.compositesb.2005.11.003.
[37] Xu X, Chen H, Fei B H, et al. Effects of age, particle size and moisture content on physical and mechanical properties of moso bamboo non-glue bonded composites. J Forest Eng, 2023; 8(1): 30-37. https://doi.org/10.13360/j.issn.2096-1359.202204036.
[38] Li HT, Xue X, Xiong ZH, Ashraf M, Lorenzo R, Shuchi S. Application case of laminated bamboo lumber structure – Building of Sentai Bamboo Research Center. Sustain Struct 2024; 4(1): 000043. https://doi.org/10.54113/j.sust.2024.000043.
[39] Xue X, Zhou W, Sayed U, et al. Design and construction of "Bamboo Cubic" facade with laminated bamboo lumber. Sustain Struct, 2023; 3(2): 000030. https://doi.org/10.54113/j.sust.2023.000030.
[40] Li H, Feng Z, Shen X, et al. Engineered bamboo bridge structure-Report on 3rd International Collaboration on Bamboo Construction. Sustain Struct, 2024; 4(3): 000062. https://doi.org/10.54113/j.sust.2024.000062.
[41] Wang Z, Wei Y, Li N, Zhao K, Ding M. Flexural behavior of bamboo–concrete composite beams with perforated steel plate connections. J Wood Sci 2020; 66, 4. https://doi.org/10.1186/s10086-020-1854-9.
[42] Lv QF, Liu Y. Experimental study on the mechanical behavior of BFRP-bamboo composite beam. Adv Compos Lett 2019; 28: 1–13. https://doi.org/10.1177/0963693519867335
[43] Zhang H, Li H, Corbi I, Corbi O, Wu G, Zhao C, et al. AFRP influence on parallel bamboo strand lumber beams. Sensors (Switzerland) 2018; 18: 1–15. https://doi.org/10.3390/s18092854.
[44] Li H, Wu G, Zhang Q, Deeks AJ, Su J. Ultimate bending capacity evaluation of laminated bamboo lumber beams. Constr Build Mater 2018; 160: 365–375. https://doi.org/10.1016/j.conbuildmat.2017.11.058.
[45] Wei Y, Ji X, Duan M, Li G. Flexural performance of bamboo scrimber beams strengthened with fiber-reinforced polymer. Constr Build Mater 2017; 142: 66–82. https://doi.org/10.1016/j.conbuildmat.2017.03.054.
[46] Baratta A, Corbi I, Corbi O. Bounds on the Elastic Brittle solution in bodies reinforced with FRP/FRCM composite provisions. Compos Part B Eng 2015; 68: 230–6. https://doi.org/10.1016/j.compositesb.2014.07.027.
[47] Li H, Li H, Hong C, Xiong Z, Lorenzo R, Corbi I, et al. Experimental investigation on axial compression behavior of laminated bamboo lumber short columns confined with CFRP. Compos Part A Appl Sci Manuf 2021; 150: 106605. https://doi.org/10.1016/j.compositesa.2021.106605.
[48] Hong C, Li H, Yang D, et al. Compressive performance of AFRP reinforced laminated bamboo stub columns. Archiv Civ Mech Eng 2022; 22, 31. https://doi.org/10.1007/s43452-021-00354-9.
[49] Yang D, Li H, Xiong Z, Mimendi L, Lorenzo R, Corbi I, et al. Mechanical properties of laminated bamboo under off-axis compression. Compos Part A Appl Sci Manuf 2020; 138: 106042. https://doi.org/10.1016/j.compositesa.2020.106042.
[50] De Lorenzis L, Rizzo A. Anchorage length of NSM FRP bars for concrete strengthening-analytical investigation and numerical modeling. ACI Structural Journal, 2004; 101(2): 269-278.
[51] Taljsten B, Carolin A, Nordin H. Concrete structures strengthened with near surface mounted reinforcement of CFRP. Adv Struct Eng 2002; 6(3): 201-213. https://doi.org/10.1260/136943303322419223.

[52] Wang Z, Li H, Fei B, Ashraf M, Xiong Z, Lorenzo R, et al. Axial compressive performance of laminated bamboo column with aramid fiber reinforced polymer. Compos Struct 2021; 258: 113398. https://doi.org/10.1016/j.compstruct.2020.113398.
[53] Micelli F, Scialpi V, La Tegola A. Flexural Reinforcement of Glulam Timber Beams and Joints with Carbon Fiber-Reinforced Polymer Rods. J Compos Constr 2005; 9: 337–347. https://doi.org/10.1061/(asce)1090-0268(2005)9:4(337).
[54] Vahedian A, Shrestha R, Crews K. Experimental and analytical investigation on CFRP strengthened glulam laminated timber beams: Full-scale experiments. Compos Part B Eng 2019; 164: 377–389. https://doi.org/10.1016/j.compositesb.2018.12.007.
[55] Wei Y, Yan S, Zhao K, Dong F, Li G. Experimental and theoretical investigation of steel-reinforced bamboo scrimber beams. Eng Struct 2020; 223: 111179. https://doi.org/10.1016/j.engstruct.2020.111179.
[56] Mostafa NH, Ismarrubie ZN, Sapuan SM, Sultan MTH. Effect of fabric biaxial prestress on the fatigue of woven E-glass/polyester composites. Mater Des 2016; 92: 579–589. https://doi.org/10.1016/j.matdes.2015.12.109.
[57] Mostafa NH, Ismarrubie ZN, Sapuan SM, Sultan MTH. The influence of equi-biaxially fabric prestressing on the flexural performance of woven E-glass/polyester-reinforced composites. J Compos Mater 2016; 50: 3385–3393. https://doi.org/10.1177/0021998315620478.
[58] Lv Q, Liu Y, Ding Y. Analyses on Prestress Loss and Flexural Performance of the Laminated Bamboo Beam Applied with Prestressed BFRP Sheet. Adv Civ Eng 2019; 2019. https://doi.org/10.1155/2019/2319814.
[59] De Luca V, Marano C. Prestressed glulam timbers reinforced with steel bars. Constr Build Mater 2012; 30: 206–17. https://doi.org/10.1016/j.conbuildmat.2011.11.016.
[60] Yang H, Ju D, Liu W, Lu W. Prestressed glulam beams reinforced with CFRP bars. Constr Build Mater 2016; 109: 73–83. https://doi.org/10.1016/j.conbuildmat.2016.02.008.
[61] ASTM D143, Standard Test Methods for Small Clear Specimens of Timber. ASTM International, West Conshohocken, PA, 2007.
[62] GB/T50329-2012. Standard for test methods of timber structures. Ministry of housing and urban-rural development of the people's Republic of China, 2012.
[63] GB/T 14017-2009. Test method for transverse grain tensile strength of wood. State Forestry Administration, 2009.
[64] GB/T 3354-1999, Test method for tensile properties of oriented fiber reinforced plastics. Beijing: China Standard Press, 1999.
[65] Zhang H, Li H, Hong C, Xiong Z, Lorenzo R, Corbi I, et al. Size Effect on the Compressive Strength of Laminated Bamboo Lumber. J Mater Civ Eng 2021; 33: 1–12. https://doi.org/10.1061/(asce)mt.1943-5533.0003776.
[66] Tian LM, Kou YF, Hao JP. Flexural behavior of sprayed lightweight composite mortar-original bamboo composite beams: Experimental study. BioResources 2019; 14: 500–517. https://doi.org/10.15376/biores.14.1.500-517.
[67] Shi B, Zhu W, Yang H, Liu W, Tao H, Ling Z. Experimental and theoretical investigation of prefabricated timber-concrete composite beams with and without prestress. Eng Struct 2020; 204: 109901. https://doi.org/10.1016/j.engstruct.2019.109901.
[68] Rahman S A, Ashraf M, Subhani M, Reiner J. Comparison of continuum damage models for nonlinear finite element analysis of timber under tension in parallel and perpendicular to grain directions. Eur J Wood Wood Prod 2022; 80(4): 771-790. https://doi.org/10.1007/s00107-022-01820-8
[69] Sandhaas C, Sarnaghi A K, van de Kuilen J W. Numerical modelling of timber and timber joints: computational aspects. Wood Sci Technol 2020; 54: 31-61. https://doi.org/10.1007/s00226-019-01142-8
[70] Wang Z, Li H, Yang D, Xiong Z, Sayed U, Lorenzo R, Corbi I, Corbi O, Hong C. Bamboo node effect on the tensile properties of side press-laminated bamboo lumber. Wood Sci Technol 2021; 55: 195-214.
[71] Li H, Gao T, Cheng G, et al. Pin groove compressive performance of laminated bamboo lumber at different angles. Cellulose, 2023; 30, 557–573. https://doi.org/10.1007/s10570-022-04920-z
[72] Ren W, Sneed L H, Yang Y, He R. Numerical simulation of prestressed precast concrete bridge deck panels using damage plasticity model. Int J Concr Struct M 2015; 9(1): 45-54. https://doi.org/10.1007/s40069-014-0091-2